Stability analysis of a phase-field model of gravity-driven unsaturated flow through porous media

Luis Cueto-Felgueroso and Ruben Juanes*
Massachusetts Institute of Technology, 77 Massachusetts Avenue, Building 48-319, Cambridge, Massachusetts 02139, USA
(Received 14 November 2008; published 9 March 2009)

The formation of preferential flow paths during infiltration of water into homogeneous, dry soil is an important phenomenon whose explanation and prediction have remained elusive under the standard theories of multiphase flow in porous media. We have recently proposed a macroscopic phase-field model of unsaturated flow in porous media, which explains why such fingering occurs [L. Cueto-Felgueroso and R. Juanes, Phys. Rev. Lett. **101**, 244504 (2008)]. Here we present a linear stability analysis of the proposed model for constant-flux infiltration, which allows a quantitative description of the wetting front instability. The present analysis stresses the critical role of the initial water saturation and applied flux ratio in the asymptotic stability of the system, as well as in the transient growth of perturbations, which is consistent with the experimental evidence. The trends in the frequency and growth factor of the most unstable modes predicted by our analysis are also in quantitative agreement with experimental measurements.

DOI: 10.1103/PhysRevE.79.036301 PACS number(s): 47.56.+r, 47.54.−r, 47.20.−k, 05.60.−k

I. INTRODUCTION

Gravity-driven infiltration of water into a homogeneous layer of soil is a simple and relevant example of pattern formation in multiphase flow through porous media. Rather than a compact infiltration front, the flow is often unstable and the water invasion takes the form of preferential flow paths (fingers). Intense experimental and theoretical work on the wetting front instability was initiated in the 1970s [1–3] and has been followed by numerous measurements of finger formation and unstable gravity-driven infiltration (see, for example, [4–11]).

Despite overwhelming experimental evidence, the description of gravity-driven unsaturated flow using macroscopic mathematical models (continuum balance laws) has remained elusive. The traditional model, known as Richards' equation [12], is a mass balance equation in which the water flux is modeled by a straightforward extension of Darcy's law to unsaturated media. It accounts for gravity, capillarity, and the fact that the permeability to water is reduced because the porous medium is only partially saturated with water.

The inability of Richards' equation to explain fingered flow was explicitly conjectured, with the support of strong numerical evidence, by Eliassi and Glass [13], considering typical constitutive relations and hysteretic effects. This conjecture has been confirmed by the successive refinement of theoretical and numerical stability analysis of unsaturated flow [8,14–20]. After the most recent theoretical results [18–20], the stability of the standard model is no longer a matter of controversy: Richards' equation is unconditionally stable under both infinitesimal and finite perturbations, which includes both asymptotic (modal) and transient (non-modal) growth effects. The relevant pattern-forming physical mechanisms are therefore missing in the classical model of unsaturated flow in porous media.

Many authors have approached the wetting front instability by drawing an analogy with the two-fluid system in a Hele-Shaw cell [21], and their analyses have led to kinematic models that reproduce trends observed in the experiments, such as relations between finger width and finger tip velocity with the flow rate through the finger [3,5,22–24]. Simulation of unstable gravity flows has also been performed with modified invasion-percolation models at the pore scale [25,26].

More recently, in light of the complexity of the problem and the growing perception that the classical mathematical model is incomplete, special attention has been paid to one-dimensional (1D) experiments, aiming at an understanding of several distinctive features of the wetting front instability, most notably the observed saturation overshoot near the tip of the fingers and the critical relevance of the injected flux ratio and initial moisture content of the soil [27–30].

Several alternatives to Richards' equation have been proposed over the last decade, and most of them rely on extensions of the concepts of saturation [31,32] and macroscopic capillary pressure [19,20,32–37]. The dynamics of an invading fluid front in disordered media has also been the subject of considerable interest within the statistical physics community [38–40]. Particularly notable in the present context is the use of the phase-field framework to simulate spontaneous imbibition processes [40]. The relevant idea behind these models is the incorporation of *nonlocal* capillary effects in the macroscopic model. A fundamental drawback of these approaches is the assumption that the porous medium is either completely dry or fully saturated by water, which is not acceptable in practice.

We have recently proposed a model of unsaturated flow that captures the relevant features of gravity fingering during inflitration [41]. Our model is derived following a phase-field methodology, which extends Richards' equation with an additional term that is formally equivalent to an apparent surface tension at the wetting front. The model predicts a saturation overshoot at the tip of the fingers, a feature that is believed to be essential for the formation of fingers. Our model is similar to that describing the flow of thin films [42,43] and to phase-field models of epitaxial growth of surfaces, binary transitions, and solidification [40,44–47]

This paper presents a linear stability analysis of the proposed phase-field model. The starting point is similar to the

*juanes@mit.edu

one adopted in the context of thin film flows [43,48–50]. In a more general context, our analysis follows the recent trends in generalized hydrodynamic stability analysis, considering both modal and nonmodal effects [51–53]. The model equation is conditionally stable under infinitesimal perturbations, and the nonnormality of the linearized operator induces, for certain relevant points in parameter space, an intense transient growth of perturbations to the traveling wave solutions of the model problem. The transient growth is conjectured to play a critical role in the velocity and width of the fingers. This transient growth is, on the other hand, limited to the initial stages in the evolution of the perturbation, which suggests that the long-time finger dynamics might be well represented by the wavelengths and growth factors obtained in the eigenvalue analysis of the linearized problem. The present study predicts the observed critical role of the initial moisture content of the soil, as well as the role of the applied flux ratio on the onset of the stability, width, and velocity of the fingers. In accordance with experimental evidence (and intuition) is also the suppression of the instability induced by capillary diffusion.

The paper is organized as follows. Section II presents the mathematical model and its nondimensional form. The base solutions about which the model equation will be linearized are traveling waves, whose shape and parameter dependence is shown in Sec. III. Section IV introduces the linearized problem and its discretization as an instrumental step towards the analysis of the propagator. Finally, Sec. V presents the results of the modal and nonmodal stability analysis, and in Sec. VI we summarize the main conclusions of the present study.

II. MATHEMATICAL MODEL

Consider constant-flux infiltration into a porous medium (Fig. 1). The evolution of the system is characterized in terms of the water saturation $S \in [0,1]$—that is, the locally averaged fraction of the pore space occupied by water. It is assumed that the initial water saturation S_0 is uniform and that the infiltration rate R_F is uniformly distributed and constant in time. The x-spatial coordinate points downwards, in the direction of gravity (acceleration g). The water density and dynamic viscosity are ρ and μ. The relevant macroscopic parameters concerning the porous medium are its intrinsic permeability k and its porosity ϕ. The permeability of the medium is often expressed as a saturated hydraulic conductivity $K_s = k\rho g/\mu$, which equals the gravity-driven flux under full saturation. Hence, the infiltration rate R_F may be expressed as a flux ratio $R_s = R_F/K_s$, with $R_s \in [0,1]$. When this idealized flow scenario is simulated experimentally, the stability of the wetting front seems to be controlled by the flux ratio, initial saturation, and material nonlinearity [36]. A saturation overshoot is observed at the tip of the fingers, which grow as traveling waves, advancing with constant velocity [54]. The formation of fingers appears as a winner-takes-all process, by which the fastest-growing fingers in the initial unstable front channelize most of the infiltrating fluid and inhibit the growth of other incipient fingers [5,54]. The initial moisture content plays a critical role in the fingering instability: even relatively low saturations lead to a compact, downward-moving wetting front [55]. Stable fronts are also observed in dry media when the infiltration rate is either very small or approaches the saturated conductivity. In general, larger infiltration rates produce faster, thicker fingers [5].

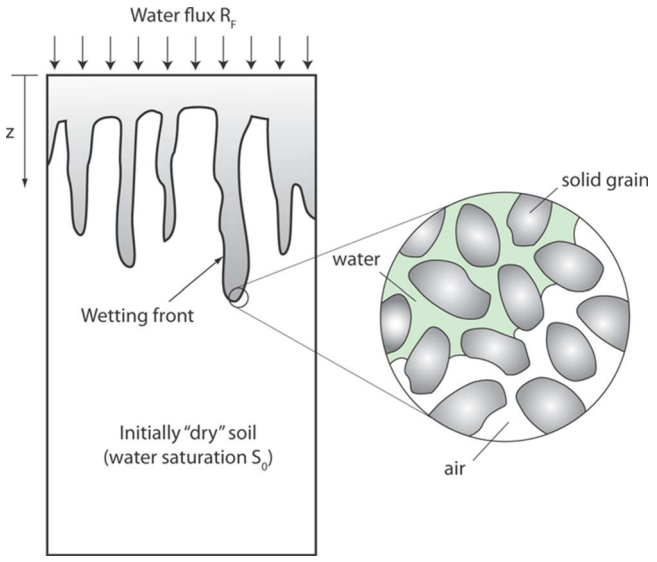

FIG. 1. (Color online) Schematic of vertical infiltration of water into a porous medium. Initially, the soil is almost dry (water saturation S_0). A constant and uniformly distributed flux of water $R_F(\mathrm{LT}^{-1})$ is allowed to infiltrate into the soil. The flux of water is less than the hydraulic conductivity of the soil, K_s, so that the flux ratio $R_s = R_F/K_s < 1$. Macroscopically, a diffuse interface (the wetting front) moves downwards. This interface is often unstable and takes the form of long and narrow fingers that travel faster than the base of the wetting front (see, e.g., Fig. 2 in [5]). Microscopically, a sharp interface between water and air exists (see inset), which is locally governed by capillary effects.

A. Phase-field model of unsaturated flow

Water mass conservation leads to an evolution equation for the water saturation S:

$$\frac{\partial(\rho\phi S)}{\partial t} + \nabla \cdot \mathbf{J} = 0, \tag{1}$$

where $\mathbf{J}$ is the water mass flux. We adopt a gradient flow formulation (see, e.g., [47]),

$$\mathbf{J} = -\rho\lambda \nabla \Phi, \tag{2}$$

where λ is the water mobility and Φ is the flow potential. The water mobility includes the effect of reduced permeability to water due to partial saturation and takes the form

$$\lambda = \frac{k}{\mu} k_r(S), \tag{3}$$

where k_r is the relative permeability to water—an increasing and typically convex function of water saturation [12,56].

Under unsaturated conditions (water saturation strictly less than 1), it is well justified to make two assumptions [56,57]. First, air is infinitely mobile compared to water and,

as a result, the air pressure remains constant and equal to atmospheric pressure. The water pressure is then equal to the negative suction (or capillary pressure):

$$p_{\text{water}} = \underbrace{p_{\text{air}}}_{=0} - P_c(S). \tag{4}$$

The capillary pressure is a monotonically decreasing but nonconvex function of water saturation [56]. The second assumption is that the compressibility of water and rock are negligible compared to that of air and, therefore, the water density ρ and the porosity ϕ are constant.

Under these conditions, we write the free energy per unit volume of the system as

$$\mathcal{E} = \mathcal{E}_{\text{gr}} + \mathcal{E}_{\text{cap}} + \mathcal{E}_{\text{nl}} = \underbrace{-\rho g S x + \Psi(S)}_{\text{local}} + \underbrace{\frac{1}{2}\Gamma|\nabla S|^2}_{\text{nonlocal}}, \tag{5}$$

which comprises the gravitational ($\mathcal{E}_{\text{gr}}$) and capillary pressure ($\mathcal{E}_{\text{cap}}$) energy potentials, as well as a nonlocal energy potential ($\mathcal{E}_{\text{nl}}$). The capillary pressure function is derived from the capillary potential:

$$P_c(S) = -\frac{d\Psi}{dS}. \tag{6}$$

The nonlocal term models the extra energetic cost associated with the displacement of water-air interfaces in areas of large saturation gradients. The coefficient Γ plays the role of an apparent surface tension associated with the wetting front [23,24,42].

The flow potential Φ is the variational derivative of the free energy:

$$\Phi = \frac{\delta \mathcal{E}}{\delta S} = \frac{\partial \mathcal{E}}{\partial S} - \boldsymbol{\nabla} \cdot \left(\frac{\partial \mathcal{E}}{\partial \boldsymbol{\nabla} S} \right) = -\rho g x - P_c(S) - \Gamma \Delta S. \tag{7}$$

Combining Eqs. (1), (2), and (7) and the unsaturated flow assumptions of constant water density and porosity, we arrive at the proposed model equation

$$\phi \frac{\partial S}{\partial t} + \boldsymbol{\nabla} \cdot \left[\frac{k\rho g}{\mu} k_r(S) \left(\boldsymbol{\nabla} x + \frac{1}{\rho g} \boldsymbol{\nabla} P_c(S) + \frac{\Gamma}{\rho g} \boldsymbol{\nabla} (\Delta S) \right) \right] = 0. \tag{8}$$

Our model is similar to that describing the flow of thin films [42,43] and to phase-field models of epitaxial growth of surfaces and binary transitions [40,47]. The traditional Richards' equation can be recovered by neglecting the nonlocal energy term in Eq. (8).

B. Nondimensional form of the equations

We nondimensionalize the model by selecting an arbitrary length scale L and a characteristic time $T = \phi L \mu / (\rho g k) = \phi L / K_s$. The capillary pressure is expressed as

$$P_c(S) = \rho g h_{\text{cap}} J(S), \tag{9}$$

where $J(S)$ is a dimensionless capillary pressure function and h_{cap} is the capillary rise, whose dependence on the system parameters is given by the Leverett scaling [58]:

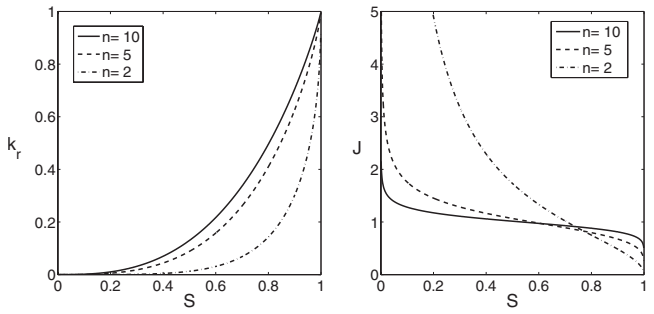

FIG. 2. Constitutive relations: relative permeability (left) and Leverett's J function (right), as given by Van Genuchten's model.

$$h_{\text{cap}} \sim \frac{\gamma \cos\theta}{\rho g \sqrt{k/\phi}}, \tag{10}$$

where γ is the surface tension between the fluids and θ is the contact angle between the air-water interface and the solid surface [59].

We define the following two nondimensional groups:

$$N_{\text{gr}} = \frac{L}{h_{\text{cap}}} \quad \text{(gravity number)}, \tag{11}$$

$$N_{\text{nl}} = \frac{\Gamma}{\rho g L^3} \quad \text{(nonlocal number)}. \tag{12}$$

With these definitions and understanding the space and time coordinates (x,t) as their dimensionless counterparts, the model reads

$$\frac{\partial u}{\partial t} + \boldsymbol{\nabla} \cdot \{k_r(u)[\boldsymbol{\nabla} x + N_{\text{gr}}^{-1} \boldsymbol{\nabla} J(u) + N_{\text{nl}} \boldsymbol{\nabla} (\Delta u)]\} = 0, \tag{13}$$

where we have used $u \equiv S$ to emphasize that the problem is expressed in nondimensional form. The functional forms of the relative permeability and capillary pressure constitutive relations are chosen to fit experimental data from quasistatic experiments. In the following, we adopt the van Genuchten-Mualem model [60,61]:

$$k_r(u) = \sqrt{u}[1 - (1 - u^{1/m})^m]^2, \tag{14}$$

$$J(u) = (u^{-1/m} - 1)^{1/n}, \tag{15}$$

where $m = 1 - 1/n$. This model introduces the material parameter n, which depends on how well sorted the porous medium is [61]. These functions are plotted in Fig. 2 for different values of n.

III. BASE SOLUTIONS AND PARAMETER DEPENDENCE

A. Traveling wave solutions

The basic states for the stability analysis of constant-flux infiltration are traveling wave solutions to (13) of the form

$$u(x,y,z,t) = u(\xi) = u(x - ct), \tag{16}$$

whose mere existence we conjecture, subject to the conditions at infinity:

$$u|_{\xi\to-\infty} = u^-, \quad u|_{\xi\to+\infty} = u^+. \tag{17}$$

The wave speed c is given by

$$c = \frac{k_r(u^-) - k_r(u^+)}{u^- - u^+}. \tag{18}$$

Let us assume that all the derivatives of the traveling waves vanish as $\xi\to\pm\infty$. With gravity acting along the x axis, the traveling wave solutions satisfy the ordinary differential equation (ODE)

$$-c\frac{du}{d\xi} + \frac{d}{d\xi}\left(k_r(u) + N_{\mathrm{gr}}^{-1}k_r(u)J'\frac{du}{d\xi} + N_{\mathrm{nl}}k_r(u)\frac{d^3u}{d\xi^3}\right) = 0. \tag{19}$$

Integrating once and imposing the necessary conditions at infinity, we arrive at

$$-c(u-u^-) + k_r(u) - k_r(u^-) + N_{\mathrm{gr}}^{-1}k_r(u)J'\frac{du}{d\xi} + N_{\mathrm{nl}}k_r(u)\frac{d^3u}{d\xi^3} = 0, \tag{20}$$

with boundary conditions

$$u|_{\xi\to-\infty} = u^-, \quad u|_{\xi\to+\infty} = u^+, \quad \left.\frac{du}{d\xi}\right|_{\xi\to-\infty} = 0. \tag{21}$$

In practical applications, the asymptotic left state u^- is expressed as a flux ratio $R_s = k_r(u^-)$ and the asymptotic right state u^+ denotes an initial water saturation of the porous medium, S_0. The nonlinear boundary-value problem (20) and (21) may be solved numerically on a suitably large domain, to obtain the 1D profiles of the base states for our stability analysis, u_0. In the present study the numerical algorithm is a rational pseudospectral method with adaptively transformed Chebyshev nodes [62,63].

B. Sample traveling wave solutions and parameter dependence

The traveling wave solutions satisfying (20) and (21) represent water saturation profiles of compact infiltration fronts. Their most salient feature is a pronounced, low-frequency overshoot upstream of the wetting front and a smaller undershoot immediately downstream. This saturation overshoot has been consistently found in experimental observations [6,30] and is believed to play a critical role in the onset of fingering instabilities. Figure 3 shows a typical traveling wave, computed using $N_{\mathrm{nl}}=1$, $N_{\mathrm{gr}}^{-1}=0.1$, $u^-=0.6$, $u^+=0.001$, and $n=10$. The small undershoot downstream of the wetting front poses a challenge from the numerical perspective of the stability analysis, since capturing this subtle feature is essential to determine the spectral properties of the linearized operator.

As N_{nl} is increased, the characteristic length scale of the overshoot also increases, accompanied by an asymptotically vanishing growth of the maximum saturation at the tip [Fig. 4(a)]. The height-to-width ratio of the bump correlates with the stability properties of the infiltration front.

The initial water saturation u^+ has been identified as a critical parameter for the onset and suppression of the fingering instability, as even small initial water contents lead to compact infiltration fronts. From the perspective of the traveling waves, the size of the overshoot reduces drastically as the initial saturation is increased, as depicted in Fig. 4(b).

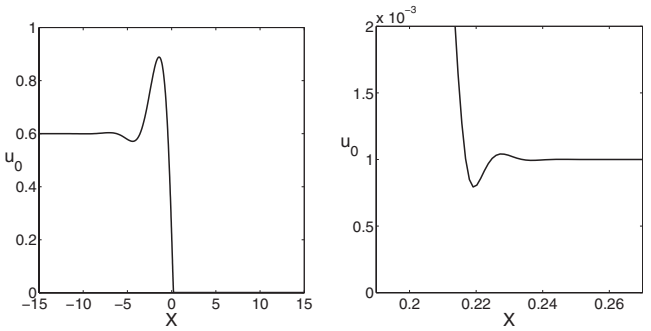

FIG. 3. Typical traveling wave solution of (13), obtained with $N_{\mathrm{nl}}=1$, $N_{\mathrm{gr}}^{-1}=0.1$, $u^-=0.6$, $u^+=0.001$, and $n=10$. Water saturation profile (left) and close-up view of the wetting front region (right).

The amount of capillary diffusion also affects the stability of the wetting front. Accordingly, higher values of N_{gr}^{-1} lead to less pronounced overshoots [Fig. 4(c)]. Finally, the infiltrating flux ratio R_s, measured here in terms of the corresponding asymptotic left state of the water saturation u^-, $R_s = k_r(u^-)$, also has a strong influence on the saturation overshoot near the wetting front. More specifically, the overshoot vanishes as $R_s\to 0$ [Fig. 4(d)]. Intense saturation at the front

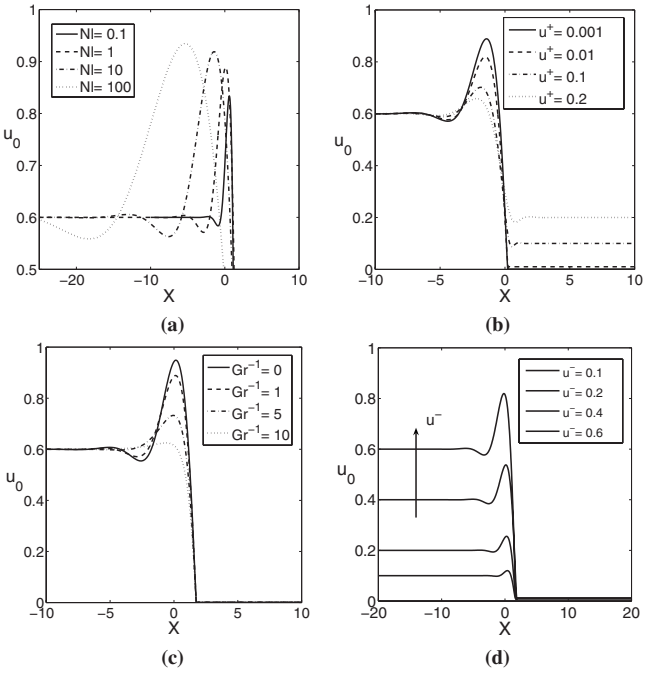

FIG. 4. (a) Influence of N_{nl} on the traveling waves. The other parameters are fixed: $N_{\mathrm{gr}}^{-1}=0.1$, $u^-=0.6$, $u^+=0.001$, and $n=10$. (b) Influence of the initial water saturation u^+ on the traveling waves. The other parameters are fixed: $N_{\mathrm{nl}}=1$, $N_{\mathrm{gr}}^{-1}=0.1$, $u^-=0.6$, and $n=10$. (c) Influence of the gravity number N_{gr} on the traveling waves. The other parameters are fixed: $N_{\mathrm{nl}}=1$, $u^-=0.6$, $u^+=0.001$, and $n=10$. (d) Influence of the flux ratio $R_s=k_r(u^-)$ on the traveling waves. The other parameters are fixed: $N_{\mathrm{nl}}=1$, $N_{\mathrm{gr}}^{-1}=1$, $n=10$, and $u^+=0.001$.

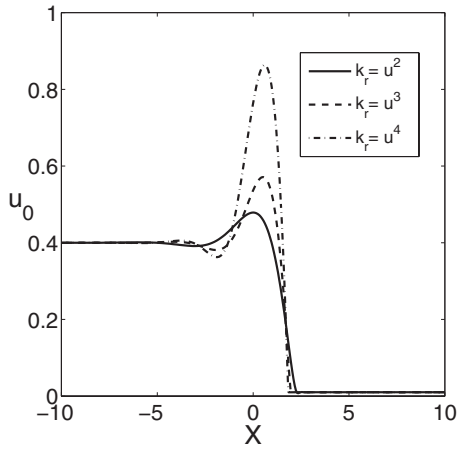

FIG. 5. Influence of the relative permeability function $k_r(u)$ on the traveling waves. The other parameters are fixed: $N_{\mathrm{gr}}^{-1}=1$, $N_{\mathrm{nl}}=1$, $u^-=0.6$, and $u^+=0.01$.

may also be triggered by the water conductivity function [the relative permeability $k_r(u)$]: highly nonlinear materials are characterized by larger overshoots (Fig. 5).

IV. LINEAR STABILITY ANALYSIS: FORMULATION AND DISCRETE OPERATORS

A. Linearized flow equation

Consider perturbations of the base traveling wave solutions u_0 developed in the previous section, of the form

$$u(x,y,t)=u_0+\epsilon g(x,y,t), \tag{22}$$

where $g(x,y,t)$ is a generic 2D perturbation of order $O(1)$ and $\epsilon \ll 1$. Introducing the above perturbed solution in (13) and retaining terms that are at most $O(\epsilon)$, the evolution equation for the perturbation is, to first order in ϵ,

$$\frac{\partial g}{\partial t}+\frac{\partial}{\partial x}(k_r' g)+N_{\mathrm{gr}}^{-1}\nabla\cdot[k_r J'\nabla g+k_r J'' g\nabla u_0+k_r' J' g\nabla u_0]+N_{\mathrm{nl}}\nabla\cdot[k_r\nabla\Delta g+k_r' g\nabla\Delta u_0]=0, \tag{23}$$

where it is understood that $k_r=k_r(u_0)$, $k_r'=k_r'(u_0)$, $J'=J'(u_0)$, and $J''=J''(u_0)$. For convenience, let us use the notation

$$T_1=N_{\mathrm{gr}}^{-1}\nabla\cdot[k_r J'\nabla g+k_r J'' g\nabla u_0+k_r' J' g\nabla u_0],$$

$$T_2=N_{\mathrm{nl}}\nabla\cdot[k_r\nabla\Delta g+k_r' g\nabla\Delta u_0]. \tag{24}$$

The above expressions can be rearranged as

$$T_1=N_{\mathrm{gr}}^{-1}\{g\nabla\cdot(k_r J''\nabla u_0+k_r' J'\nabla u_0)+[\nabla(k_r J')+k_r J''\nabla u_0+k_r' J'\nabla u_0]\cdot\nabla g+k_r J'\Delta g\} \tag{25}$$

and

$$T_2=N_{\mathrm{nl}}[g\nabla\cdot(k_r'\nabla\Delta u_0)+(k_r'\nabla\Delta u_0)\cdot\nabla g+(\nabla k_r)\cdot(\nabla\Delta g)+k_r\nabla\cdot(\nabla\Delta g)]. \tag{26}$$

Note that the base solution is constant along the y axis; i.e., $u_0=u_0(\xi)$, where $\xi=x-ct$. Therefore $u_0=u_0(x)$ in a reference frame moving with the speed c, and (25) and (26) can be rearranged as

$$T_1=N_{\mathrm{gr}}^{-1}\left[g\frac{d}{dx}\left(k_r J''\frac{du_0}{dx}+k_r' J'\frac{du_0}{dx}\right)+\left(\frac{d}{dx}(k_r J')+k_r J''\frac{du_0}{dx}+k_r' J'\frac{du_0}{dx}\right)\frac{\partial g}{\partial x}+k_r J'\Delta g\right] \tag{27}$$

and

$$T_2=N_{\mathrm{nl}}\left[g\frac{d}{dx}\left(k_r'\frac{d^3u_0}{dx^3}\right)+\left(k_r'\frac{d^3u_0}{dx^3}\right)\frac{\partial g}{\partial x}+\frac{dk_r}{dx}\left(\frac{\partial^3 g}{\partial x^3}+\frac{\partial^3 g}{\partial x\partial y^2}\right)+k_r\left(\frac{\partial^4 g}{\partial x^4}+2\frac{\partial^4 g}{\partial x^2\partial y^2}+\frac{\partial^4 g}{\partial y^4}\right)\right]. \tag{28}$$

Within the aforementioned reference frame and transforming to Fourier space in the y direction, the evolution equation for the y-transformed perturbation $G(x,\omega,t)$ is given by

$$\frac{\partial G}{\partial t}+G\frac{dk_r'}{dx}+\frac{\partial G}{\partial x}(k_r'-c)+\widehat{T_1}+\widehat{T_2}=0, \tag{29}$$

where

$$\widehat{T_1}=N_{\mathrm{gr}}^{-1}\left[G\frac{d}{dx}\left(k_r J''\frac{du_0}{dx}+k_r' J'\frac{du_0}{dx}\right)+\left(\frac{d}{dx}(k_r J')+k_r J''\frac{du_0}{dx}+k_r' J'\frac{du_0}{dx}\right)\frac{\partial G}{\partial x}+k_r J'\frac{\partial^2 G}{\partial x^2}-\omega^2 k_r J' G\right] \tag{30}$$

and

$$\widehat{T_2}=N_{\mathrm{nl}}\left[G\frac{d}{dx}\left(k_r'\frac{d^3u_0}{dx^3}\right)+\left(k_r'\frac{d^3u_0}{dx^3}\right)\frac{\partial G}{\partial x}+\frac{dk_r}{dx}\left(\frac{\partial^3 G}{\partial x^3}-\omega^2\frac{\partial G}{\partial x}\right)+k_r\left(\frac{\partial^4 G}{\partial x^4}-2\omega^2\frac{\partial^2 G}{\partial x^2}+\omega^4 G\right)\right]. \tag{31}$$

Rearranging (29), we finally arrive at the linear evolution problem

$$\frac{\partial G}{\partial t}+A_4\frac{\partial^4 G}{\partial x^4}+A_3\frac{\partial^3 G}{\partial x^3}+A_2\frac{\partial^2 G}{\partial x^2}+A_1\frac{\partial G}{\partial x}+A_0 G=0, \tag{32}$$

where

$$A_0=\frac{d}{dx}\left[k_r'+N_{\mathrm{gr}}^{-1}\left(k_r J''\frac{du_0}{dx}+k_r' J'\frac{du_0}{dx}\right)+N_{\mathrm{nl}}k_r'\frac{d^3u_0}{dx^3}\right]-N_{\mathrm{gr}}^{-1}\omega^2 k_r J'+N_{\mathrm{nl}}\omega^4 k_r, \tag{33}$$

$$A_1 = (k_r' - c) + N_{\mathrm{gr}}^{-1}\left(\frac{d}{dx}(k_r J') + k_r J'' \frac{du_0}{dx} + k_r' J' \frac{du_0}{dx}\right) + N_{\mathrm{nl}}\left(k_r' \frac{d^3 u_0}{dx^3} - \omega^2 \frac{dk_r}{dx}\right), \tag{34}$$

$$A_2 = N_{\mathrm{gr}}^{-1} k_r J' - 2N_{\mathrm{nl}}\omega^2 k_r, \tag{35}$$

$$A_3 = N_{\mathrm{nl}} \frac{dk_r}{dx}, \tag{36}$$

$$A_4 = N_{\mathrm{nl}} k_r. \tag{37}$$

B. Discretization: Asymptotic and transient growth

1. Discrete operators

The properties of the linear operator in Eq. (32) determine the evolution of infinitesimal perturbations of the base traveling wave solutions u_0. The evolution equation (32) can be discretized in the coordinate direction x, and the stability of the linearized perturbed flow can be studied in terms of the resulting discrete linear problem. Define a computational grid $\{x_j,\ j=0,\ldots,N\}$ and its associated grid function $\{G_j,\ j=0,\ldots,N\}$, where $G_j=G(x_j)$. Define discrete differential operators, through suitable differentiation matrices $\mathbf{D}_1$, $\mathbf{D}_2$, $\mathbf{D}_3$, and $\mathbf{D}_4$ [62,63], such that

$$\mathbf{G}_1 = \mathbf{D}_1\mathbf{G},$$

$$\mathbf{G}_2 = \mathbf{D}_2\mathbf{G},$$

$$\mathbf{G}_3 = \mathbf{D}_3\mathbf{G},$$

$$\mathbf{G}_4 = \mathbf{D}_4\mathbf{G}, \tag{38}$$

where the grid functions $\{G_{\alpha j},\ j=0,\ldots,N\}$ are to be understood in the sense

$$G_{\alpha j}, \approx \left.\frac{\partial^\alpha G}{\partial x^\alpha}\right|_{x=x_j}. \tag{39}$$

Under these conditions, the semidiscrete linearized flow problem reads

$$\frac{d\mathbf{G}}{dt} = \mathbf{M}\mathbf{G}, \tag{40}$$

in terms of the linear, autonomous operator

$$\mathbf{M} = -(\mathbf{A}_4\mathbf{D}_4 + \mathbf{A}_3\mathbf{D}_3 + \mathbf{A}_2\mathbf{D}_2 + \mathbf{A}_1\mathbf{D}_1 + \mathbf{A}_0). \tag{41}$$

In the above expression, the matrices $\mathbf{A}_k$, $k=0,\ldots,4$, are diagonal, and their entries result from the evaluation of the coefficients (33)–(37) at the grid points. It follows from (40) that, given a perturbation $G(x,\omega,0)=G_0(x,\omega)$—i.e., given the grid function $\{G_{0j},\ j=0,\ldots,N\}$—the evolution of this perturbation can be compactly written as

$$\mathbf{G}(t) = e^{t\mathbf{M}}\mathbf{G}_0, \tag{42}$$

where the matrix exponential that defines the propagator is to be understood in the sense of

$$e^{t\mathbf{M}} = \sum_{k=0}^{\infty} \frac{t^k \mathbf{M}^k}{k!}. \tag{43}$$

2. Spectral characterization

We denote by $\sigma(\mathbf{M}) \in C$ the *spectrum*, or set of all the eigenvalues, of $\mathbf{M}$. For an arbitrary $\epsilon > 0$, the ϵ-*pseudospectrum* of $\mathbf{M}$, $\sigma_\epsilon(\mathbf{M})$, is defined as the set of $z \in C$ such that [53]

$$\|(z-\mathbf{M})^{-1}\| > \epsilon^{-1}. \tag{44}$$

In the above expression, and hereafter, we loosely write $(z-\mathbf{M})$ instead of $(z\mathbf{I}-\mathbf{M})$. The matrix $(z-\mathbf{M})^{-1}$ is called the *resolvent* of $\mathbf{M}$ at z. Note that $\|(z-\mathbf{M})^{-1}\| \to \infty$ for $z \in \sigma(\mathbf{M})$. In addition, let us define the spectral [ϵ-pseudospectral] *abscissa* of $\mathbf{M}$, $\alpha(\mathbf{M})$ [$\alpha_\epsilon(\mathbf{M})$], as the supremum of the real part of the spectrum [ϵ-pseudospectrum].

We are interested in the growth and decay of solutions $\mathbf{G}(t)$ to the linear time-dependent problem $d\mathbf{G}/dt = \mathbf{M}G$—i.e., $\mathbf{G}(t) = e^{t\mathbf{M}}\mathbf{G}(0)$. Asymptotically, the behavior of the system is driven by the eigenvalues of $\mathbf{M}$. More precisely,

$$\lim_{t\to\infty} t^{-1} \ln\|e^{t\mathbf{M}}\| = \alpha(\mathbf{M}). \tag{45}$$

In terms of transient growth, an eigenvalue (*modal*) analysis provides just a lower bound, as

$$\|e^{t\mathbf{M}}\| \geqslant e^{t\alpha(\mathbf{M})} \quad \forall\ t \geqslant 0. \tag{46}$$

Pseudospectra provide sharper information about the growth and decay behavior of the system for intermediate times. A simple lower bound is given by [53]

$$\sup_{t\geqslant 0}\|e^{t\mathbf{M}}\| \geqslant \frac{\alpha_\epsilon(\mathbf{M})}{\epsilon} \quad \forall\ \epsilon > 0. \tag{47}$$

The above inequality states that, even when $\alpha(\mathbf{M}) \leqslant 0$, in which case the system would be diagnosed as stable from a modal perspective, a nonmodal study may reveal intense transient growth if the ϵ-pseudospectra contours protrude significantly into the right half of the complex plane.

V. MODAL AND NONMODAL STABILITY ANALYSIS: ONSET AND SUPPRESSION OF THE FINGERING INSTABILITY

A. Eigenvalues and asymptotic growth

We start with a classical modal stability analysis. Therefore the relevant parameter to be considered at this point is the spectral abscissa of the linear operator $\mathbf{M}$. Under this perspective and for a perturbation with wave number ω, the dynamical system is said to be unstable if $\alpha(\mathbf{M}(\omega)) > 0$, which implies asymptotic exponential growth, and stable if $\alpha(\mathbf{M}(\omega)) < 0$, which dictates asymptotic exponential decay. This approach does not consider transient growth effects due to interactions between nonorthogonal eigenmodes.

Figure 6 shows the dispersion curves [growth factor $\beta = \alpha(\mathbf{M}(\omega))$ against wave number ω] for different values of

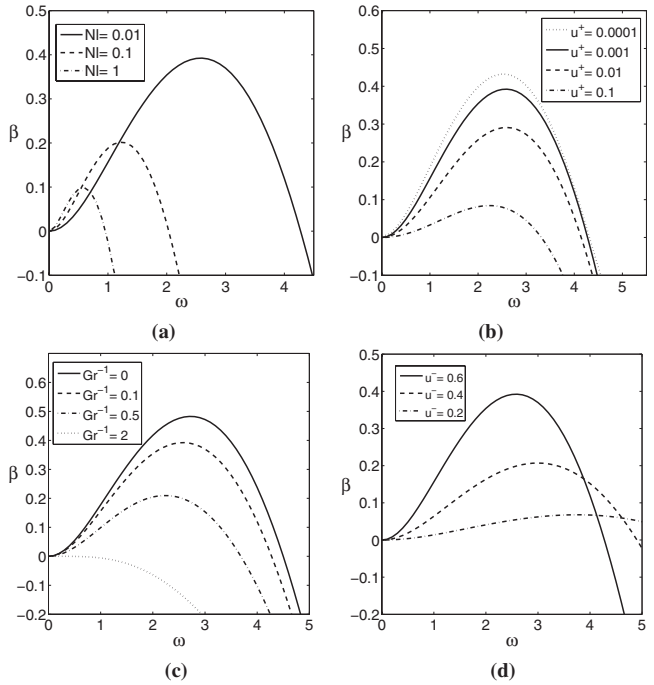

FIG. 6. Growth factor $\beta=\alpha(\mathbf{M}(\omega))$, as a function of ω. (a) Influence of the nonlocal number N_{nl}. (b) Influence of the initial water saturation u^{+}. (c) Influence of the gravity number N_{gr}. (d) Influence of the flux ratio $R_s=k_r(u^{-})$. The default parameters are $N_{\mathrm{nl}}=0.01$, $N_{\mathrm{gr}}^{-1}=0.1$, $u^{-}=0.6$, $u^{+}=0.001$, and $n=10$.

the model parameters. As the gravity number is decreased ($N_{\mathrm{gr}}\to 0$), the traveling waves are unstable for a smaller range of lower frequencies and with smaller associated growth factors [Fig. 6(c)]. This simply reflects the stabilizing effect of capillary diffusion. From the perspective of characterizing the incipient fingers, this can be interpreted as the formation of thicker, slower fingers as $N_{\mathrm{gr}}\to 0$. Increases in N_{nl} over the range $N_{\mathrm{nl}}\in[0.01,1]$ [Fig. 6(a)] show a similar trend, but now the damping of high frequencies is much more pronounced for large N_{nl}, in accordance with the powerful dissipation properties of the fourth-order term. Consistent with experimental observations, the initial water saturation has a critical effect on the instability [Fig. 6(b)]. Also in agreement with experiments, smaller flux ratios [Fig. 6(d)] give rise to thinner, slower-moving fingers. Eventually, for a sufficiently small flux ratio, the instability is suppressed. The standard Richards' model is recovered in the limit $N_{\mathrm{nl}}\to 0$. This limit corresponds also with stability of the system, as illustrated in Fig. 7, and in accordance with numerous numerical and theoretical studies of Richards' equation [18–20].

B. Pseudospectra and transient growth

The nonnormality of the linearized operator $\mathbf{M}$ in (42) can be illustrated with a simple example (Fig. 8). The model parameters are $N_{\mathrm{nl}}=10^{-3}$, $N_{\mathrm{gr}}^{-1}=0.1$, $u^{-}=0.6$, $u^{+}=0.001$, and $n=10$. An eigenvalue analysis suggests conditional stability, with unstable modes in the range $\omega\in[0,8.7]$ [Fig. 8(a)]. However, the norm of the propagator $\|\exp(t\mathbf{M})\|$ for $\omega=5.4$

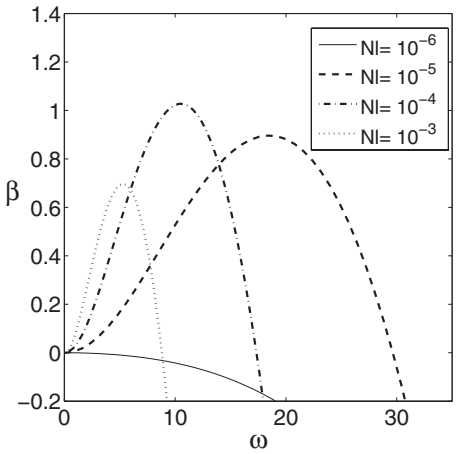

FIG. 7. Suppression of the instability in the limit $N_{\mathrm{nl}}\to 0$. The other parameters are $N_{\mathrm{gr}}^{-1}=0.1$, $u^{-}=0.6$, $u^{+}=0.001$, and $n=10$.

(nearly most unstable mode) and $\omega=9$ (asymptotically stable) reveals that, even though the asymptotic behavior is in accordance with the eigenvalue predictions, there is considerable transient growth which is not predicted by the modal analysis. Notably, the transient growth associated to the "stable" mode $\omega=9$ is similar to that of the nearly most unstable one [Fig. 8(b)]. The existence of intense transient

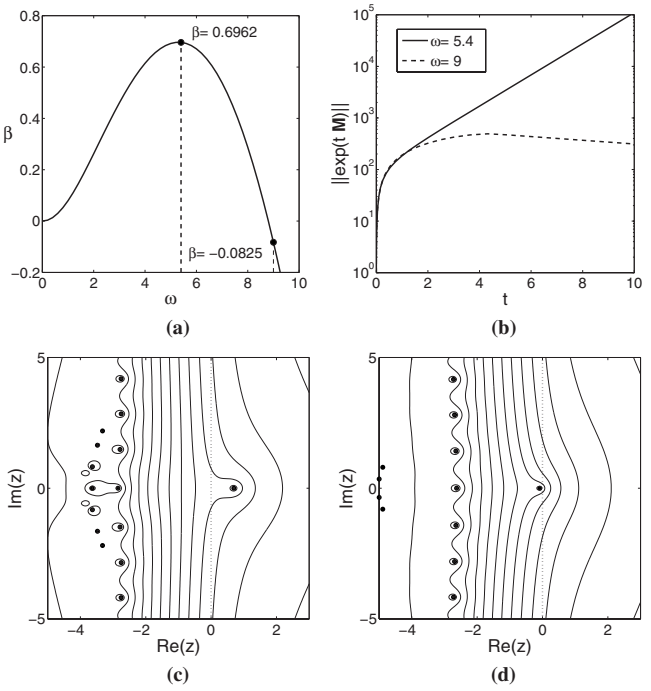

FIG. 8. Non-normal behavior of the linearized operator and transient growth. The parameters are $N_{\mathrm{nl}}=10^{-3}$, $N_{\mathrm{gr}}^{-1}=0.1$, $u^{-}=0.6$, $u^{+}=0.001$, and $n=10$. (a) Dispersion curve showing the growth factors associated to an asymptotically unstable mode ($\omega=5.4$) and an asymptotically stable mode ($\omega=9$). The transient growth of these asymptotically unstable and stable modes is nearly identical (b), which can be better understood considering their associated ϵ-pseudospectra [(c) and (d), respectively]. In the pseudospectra we plot the eigenvalues (●), as well as the contours $\epsilon=10^{-1},10^{-1.5},\ldots,10^{-8}$.

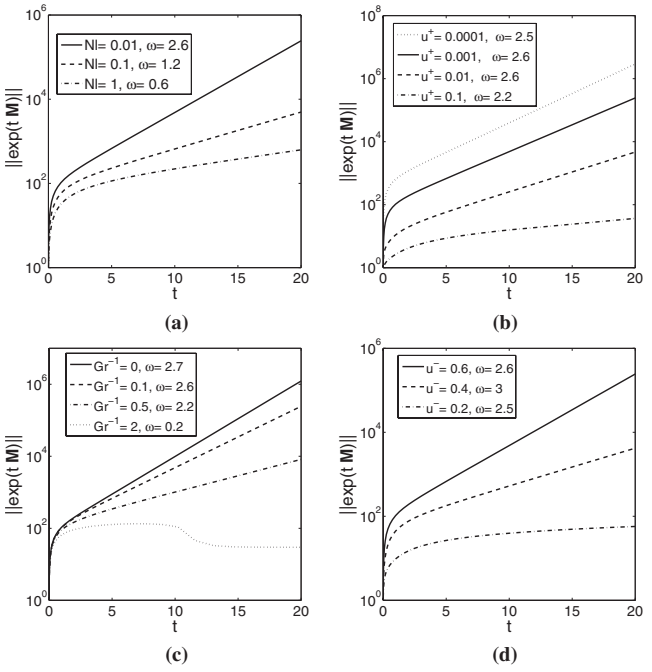

FIG. 9. (a) Influence of N_{nl} on the transient growth of perturbations of the base state. The other parameters are fixed: $N_{\mathrm{gr}}^{-1}=0.1$, $u^{-}=0.6$, $u^{+}=0.001$, and $n=10$. (d) Influence of the initial water saturation u^{+} on the transient growth of perturbations of the base state. The other parameters are fixed: $N_{\mathrm{nl}}=0.01$, $N_{\mathrm{gr}}^{-1}=0.1$, $u^{-}=0.6$, and $n=10$. (c) Influence of the gravity number N_{gr} on the transient growth of perturbations of the base state. The other parameters are fixed: $N_{\mathrm{nl}}=0.01$, $u^{-}=0.6$, $u^{+}=0.001$, and $n=10$. (b) Influence of the flux ratio (expressed in terms of u^{+}) on the transient growth of perturbations of the base state. The other parameters are fixed: $N_{\mathrm{nl}}=0.01$, $N_{\mathrm{gr}}^{-1}=0.1$, $u^{+}=0.001$, and $n=10$.

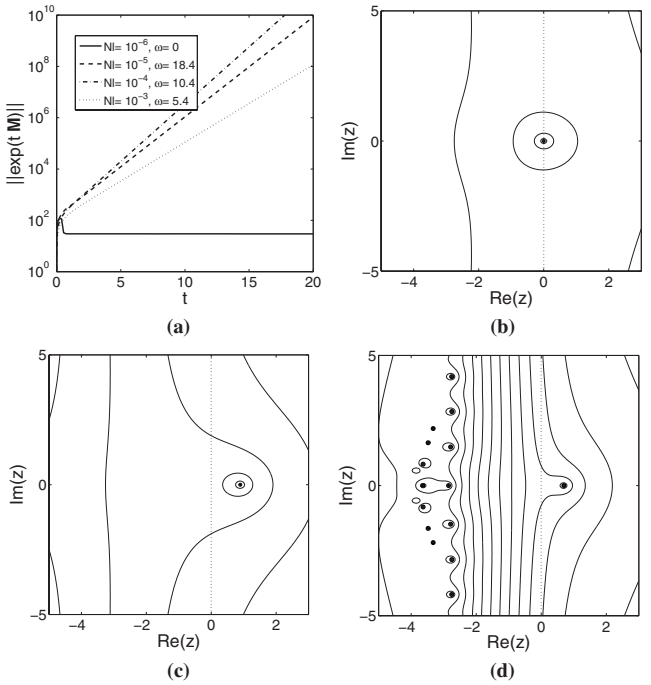

FIG. 10. Suppression of the instability as $N_{\mathrm{nl}}\rightarrow 0$. (a) Evolution of $\|\exp(t\mathbf{M})\|$ for different values of N_{nl} (most unstable modes). ϵ-pseudospectra for $N_{\mathrm{nl}}=10^{-6}$ (b), $N_{\mathrm{nl}}=10^{-5}$ (c), and $N_{\mathrm{nl}}=10^{-3}$ (d). In the pseudospectra we plot the eigenvalues (●) as well as the contours $\epsilon=10^{-1},10^{-1.5},\ldots,10^{-8}$.

growth may suggest that the conclusions derived from an asymptotic analysis of the linearized problem are somewhat misleading, as the powerful initial transients could invalidate the linearization about the basic solution.

This transient growth behavior of the propagator can be understood by looking at the pseudospectra of $\mathbf{M}(\omega)$ [Figs. 8(c) and 8(d)]. For $\omega=5.4$ [Fig. 8(c)], both the largest eigenvalue and the ϵ contours protrude significantly into the right half of the complex plane, which explains both the transient and asymptotic growth. For $\omega=9$ [Fig. 8(d)], while the largest eigenvalue has a negative real part, indicating asymptotic decay, the ϵ contours advance well into the positive half plane, indicating transient growth of the perturbations.

Figure 9 shows the transient growth behavior in terms of the system parameters. While the gravity number N_{gr} and the nonlocal number N_{nl} have a relatively modest influence on transient growth [Figs. 9(c) and 9(a), respectively], suggesting that capillary diffusion is less critical in the early stages of the perturbation growth, the initial water saturation [Fig. 9(b)] and applied flux ratio [Fig. 9(d)] seem to be fundamental parameters in the initial growth of perturbations. The approximate scaling with $(u^{+})^{-1}$ is consistent with the stability of thin film flows [43]. Experimental measurements have stressed the central role of u^{+} and u^{-} in the fingering instability.

The return to normality of the operator is obtained when the macroscopic interface effects are neglected, $N_{\mathrm{nl}}\rightarrow 0$, which corresponds to the traditional Richards' equation (Fig. 10). As N_{nl} is reduced, not only does the largest eigenvalue become smaller, and eventually negative, but also the nature of the linearized operator changes, from a typical non-normal pattern to a nearly normal behavior. Therefore, going back to the standard Richard equation implies asymptotic stability and negligible transient growth, which is consistent with recent theoretical analysis that remark the strong stability of the Richards' model and its inability to capture fingering phenomena [13,18].

C. Optimal perturbations and eigenmodes

The disturbance at $t=0$ that elicits a final state at time t with maximal growth can be determined within the linearized theory from the singular-value decomposition (SVD) of the propagator [52] according to $\exp(t\mathbf{M})=\mathbf{U}\boldsymbol{\Sigma}\mathbf{V}^{*}$. The optimal initial disturbance is the first column of $\mathbf{V}$, whereas the final evolved state is the first column of $\mathbf{U}$. The amplification factor of the optimal disturbance is the first (maximum) singular value in $\boldsymbol{\Sigma}$, in the sense that $\sigma_{max}=\|\exp(t\mathbf{M})\|$. The normalized shape of the maximal evolved disturbance for late times is given by the eigenmode associated to eigenvalue that gives the spectral abscissa of $\mathbf{M}$.

For the present study, we focus on the influence of the initial moisture content of the soil, u^{+}, on the shape of the optimal perturbations. Figure 11 depicts the normalized eigenmodes associated to increasing initial saturations—

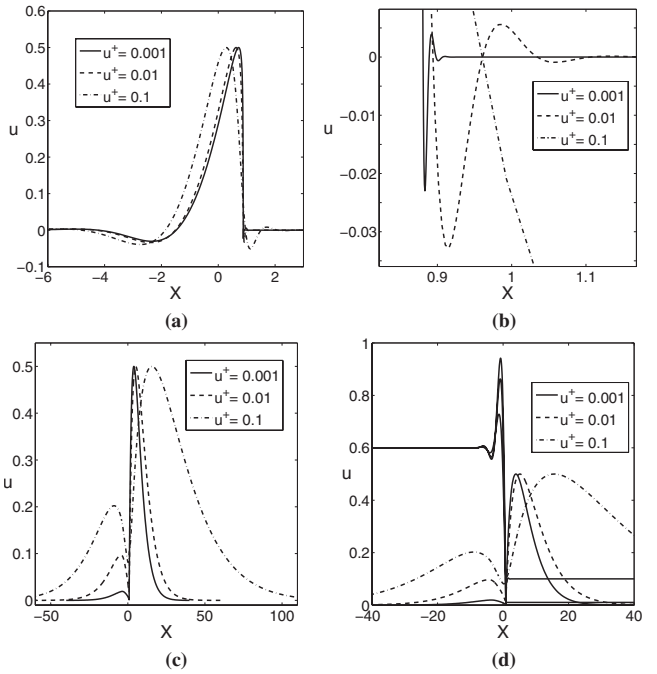

FIG. 11. (a) Comparison of the eigenmode (normalized) associated with the mode $\omega=0.6$ in terms of the initial moisture content u^+. The other parameters are $N_{\rm nl}=1$, $N_{\rm gr}^{-1}=0.1$, $u^-=0.6$, and $n=10$. (b) Close-up view of the eigenmodes in the region near the wetting front. (c) Comparison of the initial perturbation associated with the eigenmode (normalized). Model parameters as before. (d) Close-up view of the region near the wetting front. We also plot the traveling wave saturation profiles as a reference.

namely, $u^+=0.001$, $u^+=0.01$, and $u^+=0.1$ [Fig. 11(a)]—together with a close-up view of the region near the apparent wetting front [Fig. 11(b)]. As the initial moisture content is increased, the eigenmodes tend to exhibit more spreading around the front. Note that, while the eigenmodes for $u^+=0.001$ and $u^+=0.01$ are quantitatively similar, there is a pronounced difference with respect to $u^+=0.1$. The optimal initial perturbations [Figs. 11(c) and 11(d)] reflect the intense perturbation required in the case of larger initial saturations.

It is interesting to analyze the short-time growth of perturbations through the singular-value decomposition of the propagator. Figure 12 shows the normalized optimal initial perturbation with respect to $t=0.1$, as well as its normalized evolved state for $u^+=0.001$ [Figs. 12(a) and 12(b)], $u^+=0.01$ [Figs. 12(c) and 12(d)], and $u^+=0.1$ [Figs. 12(e) and 12(f)]. The base state is also included as a reference. The growth factor associated to the evolved disturbance is 5.16 for $u^+=0.001$. Note that the optimal excitation is sharply localized near the apparent wetting front. The results are similar for $u^+=0.01$, although the growth factor is reduced to 1.74. Increasing the initial saturation further results in a qualitative difference, as the initial and evolved states are nearly identical, with a growth factor of just 1.06. The obvious consequence of the analysis above is that, while for $u^+=0.001$ a small perturbation localized at the wetting front elicits a disturbance at $t=0.1$ that has traveled behind the wetting front and has grown by a factor of 5.16, for $u^+=0.1$ we need to start from a perturbation that already ex-

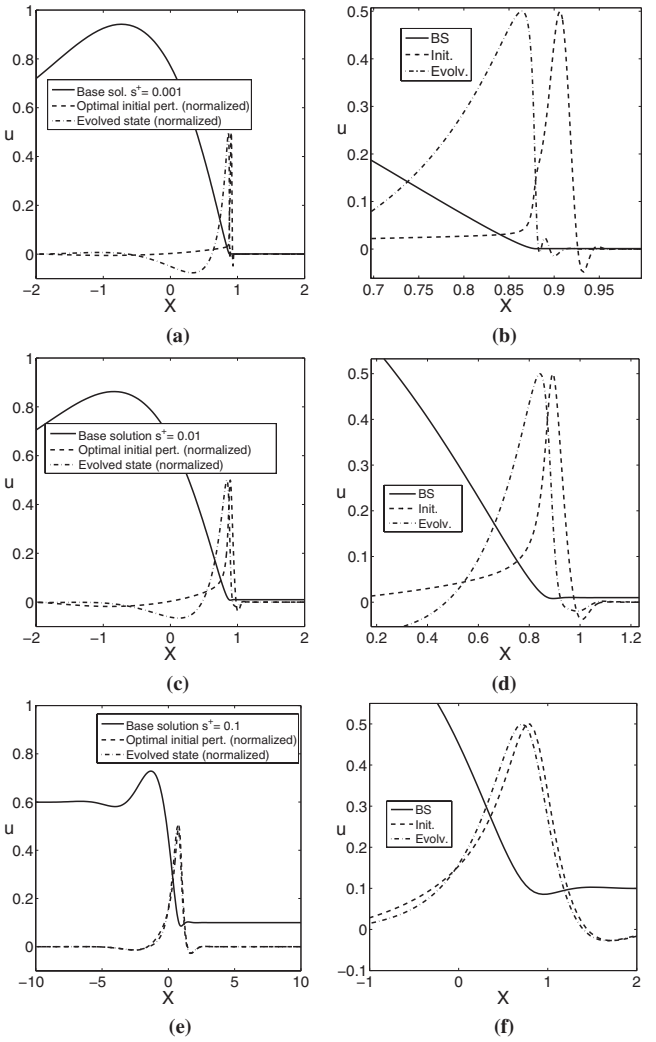

FIG. 12. Normalized optimal perturbation and evolved state for $t=0.1$ and different initial saturations: (a), (b) $u^+=0.001$, (c), (d) $u^+=0.001$, and (e), (f) $u^+=0.01$. The other parameters are $N_{\rm nl}=1$, $N_{\rm gr}^{-1}=0.1$, $u^-=0.6$, and $n=10$. Left: base flow and normalized initial and evolved state. Right: close-up view of the region near the wetting front. The growth factor of the evolved state is $\sigma_{0.001}=5.16$, $\sigma_{0.01}=1.74$, and $\sigma_{0.1}=1.06$.

tends behind the wetting front and at the same time level would have grown just by a factor of 1.06.

These results are again consistent with the fact that fingering is observed only in wetting fronts infiltrating into sufficiently dry media. The apparent wetting front acts as an amplifier (this effect has also been observed in contact lines [43]) and in such a way that for very low initial moisture contents even small perturbations ahead of the front are intensely amplified. For initially wet soils, on the other hand, the wetting front is destabilized only by significantly larger perturbations that extend over larger regions and grow more slowly, thus reducing the likelihood of fingered flow.

VI. Stability along $N_{\rm nl}=N_{\rm gr}^{-3}$

In [41], we proposed to express the dimensionless group $N_{\rm nl}$ in terms of the already considered system parameters,

thus avoiding the introduction of new independent parameters with respect to Richards' equation. The introduction of the nonlocal (gradient) term in the energy potential raises the question about the definition of the dimensionless group N_{nl}, which is formally equivalent to an apparent surface tension at the wetting front. While it is legitimate to postulate its dependence on additional intrinsic properties of the system, the idea of a nonlocal interface is fundamentally a macroscopic construct, which should depend only on the already considered basic parameters. Dimensional analysis then leads to the scaling $N_{\mathrm{nl}} \sim N_{\mathrm{gr}}^{-3}$, and we propose the simple relation

$$N_{\mathrm{nl}} = N_{\mathrm{gr}}^{-3}. \tag{48}$$

As a consequence of Eq. (48), the gravity number N_{gr} sets the intrinsic scale of the problem and the proposed model (13) contains a new term, but not a new independent parameter.

In terms of the stability of the system, the relevance of this choice becomes clear by looking at the wave number and growth factor of the most unstable modes in the N_{nl}-N_{gr} plane (Fig. 13). There is a narrow region in the parameter space N_{gr}-N_{nl} where $\omega_{\max}$ [Fig. 13(a)] and $\beta_{\max}$ [Fig. 13(b)] decay exponentially. This region of abrupt decay marks the effective transition from a compact infiltration front to fingering instability and follows a straight line (in logarithmic scale) of slope −3, which is consistent with the arbitrariness of the choice of reference length L. The specific location of this transition (not its slope) is determined by the system parameters R_s, S_0, and n. This critical region cannot be crossed when N_{gr} moves along $N_{\mathrm{nl}}=N_{\mathrm{gr}}^{-3}$, and therefore changes in the gravity number do not induce regime transition. Under the scaling $N_{\mathrm{nl}}=N_{\mathrm{gr}}^{-3}$, $\omega_{\max}$ and $\beta_{\max}$ are linear functions of N_{gr} (Fig. 14) and nonlinear functions of S_0, R_s, and n. In other words, the scale of the flow is determined by the gravity number and its nonlinear dynamics is controlled by the flux ratio, initial saturation, and constitutive relations. This linear dependence on N_{gr} is illustrated in Fig. 14.

The nonlinear dependence of the scale-invariant frequencies and growth factors, $\omega_{\max}/N_{\mathrm{gr}}$ [Fig. 13(c)] and $\beta_{\max}/N_{\mathrm{gr}}$ [Fig. 13(d)], on the flux ratio, initial saturation, and material nonlinearity, is shown in Figs. 15–17, respectively. They are indicative of the early dynamics of the perturbed flow and the properties of the emerging fingers. The onset of preferential flow paths in the unstable wetting front is more intense for larger flux ratios and smaller initial saturations [Fig. 13(d)]. For very dry media the size of the incipient fingers decreases with the flux ratio. In general, however, for each value of the initial saturation there is a critical flux ratio beyond which smaller fluxes lead to larger finger sizes [Fig. 13(c)]. The growth factor and frequency of the most unstable mode decay exponentially as the initial saturation is increased. This abrupt decay agrees with experimental observations, which have suggested the existence of critical values of S_0 for the suppression of the instability [55].

VII. DISCUSSION

We have proposed a phase-field model of unsaturated flow in porous media. The fundamental phenomenological

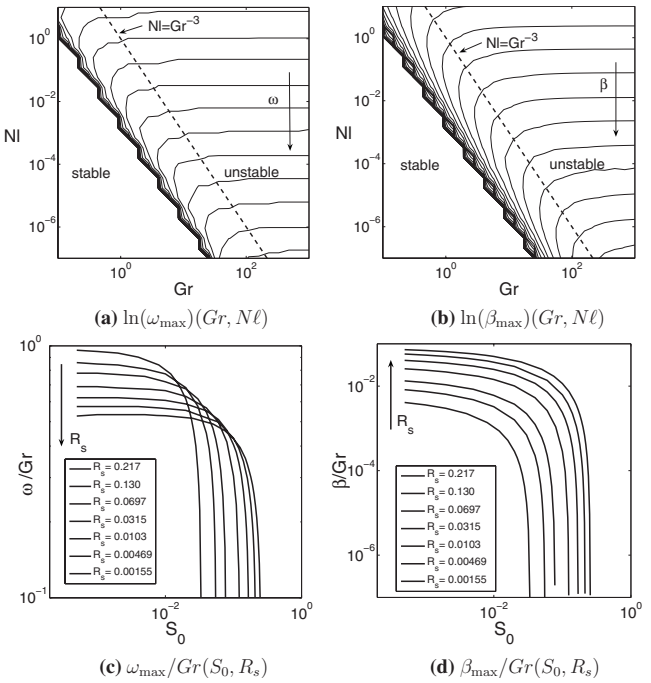

FIG. 13. Results of the linear stability analysis of Eq. (13). (a), (b) Contours of the logarithm of the frequency $\omega_{\max}$ of the most unstable mode and its associated growth factor $\beta_{\max}$, as functions of the dimensionless groups N_{gr} and N_{nl}. We set $R_s=0.217$, $S_0=0.01$, and $n=10$. A narrow region of exponential decay, along a straight line of slope −3, marks the effective transition from stable to unstable flow. The position of this transition region, not its slope, is determined by R_s, S_0, and n. Since our model assumes $N_{\mathrm{nl}}=N_{\mathrm{gr}}^{-3}$, the transition region cannot be crossed by modifying N_{gr} alone. (c) Exponential decay of the scale-invariant frequencies $\omega_{\max}/N_{\mathrm{gr}}$ with the initial saturation S_0. For a given S_0, the frequencies increase with decreasing R_s up to a critical flux beyond which $\omega_{\max}/N_{\mathrm{gr}}$ decreases again. (d) Exponential decay of the scale-invariant growth factor $\beta_{\max}/N_{\mathrm{gr}}$ with the initial saturation S_0. Within the unsaturated regime, the growth factors increase monotonically with R_s.

characteristics of the fingering instability in gravity-driven unsaturated infiltrating flow in homogenous porous media can be understood and quantified from a linear stability analysis of the model. We draw two general conclusions from our analysis.

(i) The instability is an instrinsic feature of the infiltrating wetting front. The fingering instability will develop, for suitable points in the parameter space, even for infinitesimal perturbations of a steady-state base flow within a homogeneous porous medium.

(ii) The instability is an intrisic feature of *unsaturated* flow. Thus, it is arbitrary to assume that the wetting front has to be fully saturated in order to develop instabilities.

Transient growth is fundamental in the onset of the fingering instability. In this sense, transient growth can only be relevant if small perturbations are amplified up to levels $O(1)$ within a short period of time. The maximum transient amplification depends strongly on the initial saturation of the porous medium u^+ and the applied flux ratio $R_s=k_r(u^-)$ and somewhat weakly on mild variations of other parameters like

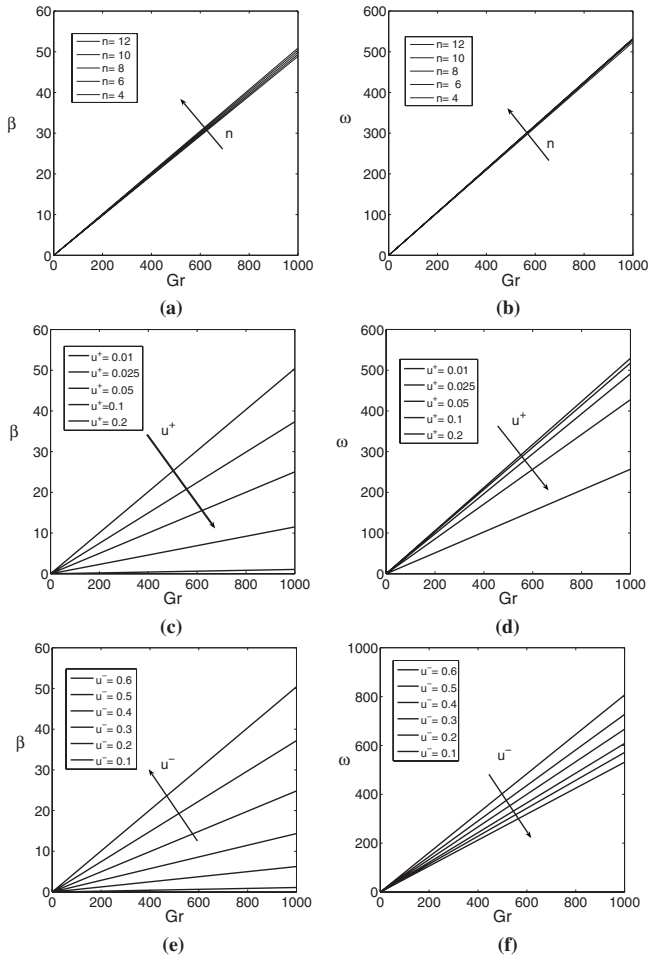

FIG. 14. Stability analysis along $N_{nl}=N_{gr}^{-3}$. Linear dependence of β_{max} [(a), (c), (e)] and ω_{max} [(b), (d), (f)] with the gravity number N_{gr}. (a), (b) Material parameter n [61]. (c), (d) Initial saturation u^+. (e), (f) Flux ratio $R_s=k_r(u^-)$.

the gravity number N_{gr} and the nonlocal number N_{nl}. This is in accordance with strong experimental evidence pointing towards the critical role of the initial saturation and flux ratio on the observed saturation overshoot and finger development. As the initial saturation increases, the amount of transient growth is reduced in such a way that only large perturbations can achieve significant amplification. Under these conditions, capillary diffusion will effectively damp perturbations, suppressing the onset of the instability. As a consequence, even relatively small initial saturations are likely to prevent the appearance of fingers for realistic values of the gravity number N_{gr}.

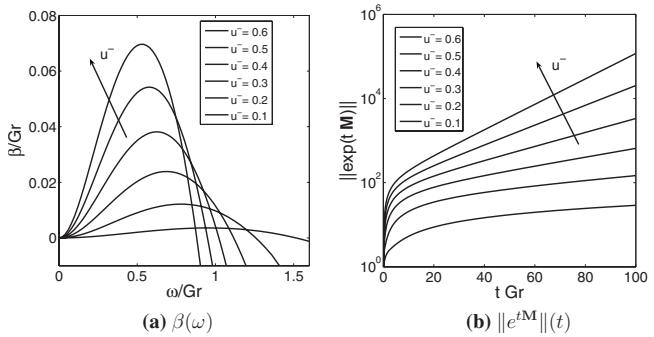

FIG. 15. Stability analysis along $N_{nl}=N_{gr}^{-3}$. Influence of the flux ratio (through the left state u^-) on the stability of the traveling wave solutions to Eq. (13). (a) Dispersion curves, plotting growth factor β/N_{gr} versus frequency of the perturbations ω/N_{gr}. (b) Transient growth of asymptotically unstable perturbations.

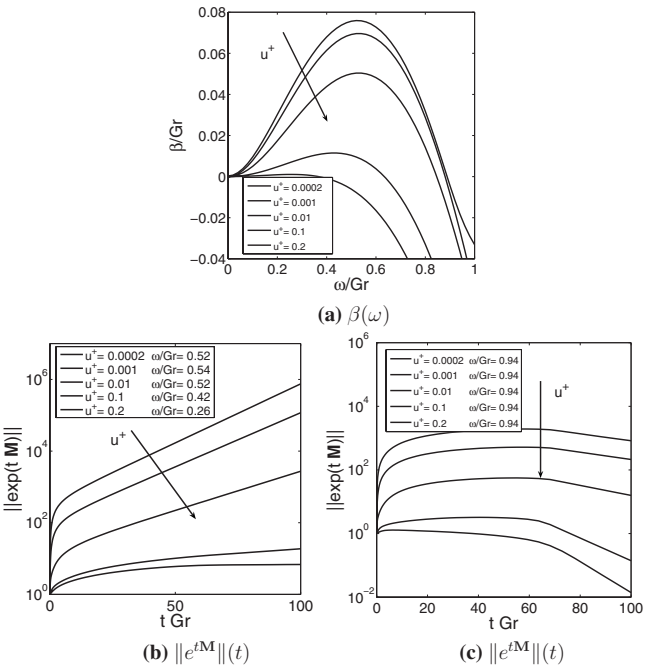

FIG. 16. Stability analysis along $N_{nl}=N_{gr}^{-3}$. Influence of the initial saturation (right state u^+) on the stability of the traveling wave solutions to Eq. (13). (a) Dispersion curves, plotting growth factor β/N_{gr} versus frequency of the perturbations ω/N_{gr}. (b) Transient growth of asymptotically unstable perturbations. (c) Transient growth of asymptotically stable perturbations.

Transient growth occurs within a short period of time, which precedes the transition to the asymptotic growth behavior, governed by the eigenvalues of the linearized system. Therefore, and in spite of possible nonlinear effects due to the interaction of nonorthogonal modes during the transient

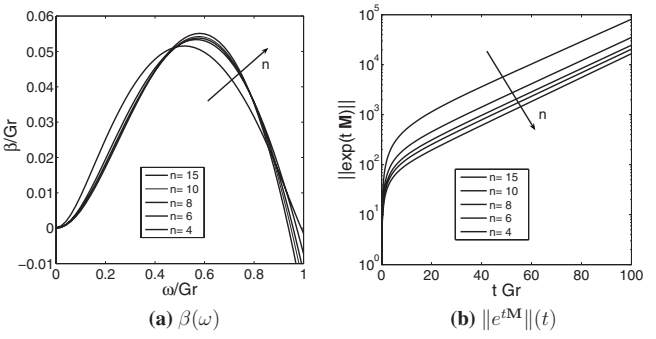

FIG. 17. Stability analysis along $N_{nl}=N_{gr}^{-3}$. Influence of the constitutive relations (through Van Genuchten's parameter n [61]) on the stability of the traveling wave solutions to Eq. (13). (a) Dispersion curves, plotting growth factor β/N_{gr} versus frequency of the perturbations ω/N_{gr}. (b) Transient growth of asymptotically unstable perturbations.

growth, the modal analysis seems to be adequate to predict the most relevant features of the late-time fingering phenomenon. This conclusion is also reinforced by the phenomenological fact that, for homogeneous, initially dry media, the instability of the wetting front adopts the form of persistent and distinctive patterns (fingers), whose width and tip velocity can be correlated to basic experimental parameters, notably the flux ratio, nonlinearity of the material, and initial moisture content. Using dimensional analysis, these correlations can be predicted through the analysis of the wavelength and growth factor of the most unstable mode for each particular point in parameter space. The predictions agree with experimental observations [41].

The key ingredient of the proposed model is the introduction of a nonlinear fourth-order term, which is formally equivalent to an apparent surface tension at the wetting front. The introduction of this term constitutes a departure from the classical Richards' equation. In addition to modeling physical mechanisms that are missing in the classical model and from a mathematical perspective, the new term in the proposed model introduces a new mechanism in the dynamics of the system: a significant degree of non-normality. Thus, in addition to the mere existence of asymptotically unstable modes, the transient growth of perturbations can be very intense depending on the parameter values and, in particular, for very dry media. We believe that this transient growth is the fundamental element to explain the appearance of fingers in practice, while a modal analysis can be used to quantitatively predict some long-time features of the developed patterns, such as finger width and finger tip velocity [41].

ACKNOWLEDGMENTS

We gratefully acknowledge funding for this research, provided by Eni under the Multiscale Reservoir Science project, and by the ARCO Chair in Energy Studies.

[1] D. Hill and J.-Y. Parlange, Soil Sci. Soc. Am. Proc. **36**, 397 (1972).
[2] J. R. Philip, Soil Sci. Soc. Am. Proc. **39**, 1042 (1975).
[3] J.-Y. Parlange and D. E. Hill, Soil Sci. **122**, 236 (1976).
[4] G. Diment and K. Watson, Water Resour. Res. **21**, 979 (1985).
[5] R. Glass, J.-Y. Parlange, and T. Steenhuis, Water Resour. Res. **25**, 1195 (1989).
[6] J. Selker, P. Leclerq, J.-Y. Parlange, and T. Steenhuis, Water Resour. Res. **28**, 2513 (1992).
[7] T. Bauters, D. DiCarlo, T. Steenhuis, and J.-Y. Parlange, J. Hydrol. **231**, 244 (2000).
[8] X. Du, T. Yao, W. Stone, and J. Hendrickx, Water Resour. Res. **37**, 1869 (2001).
[9] O. Sililo and J. Tellam, Ground Water **38**, 864 (2000).
[10] Z. Wang, A. Tuli, and W. Jury, Vadose Zone J. **2**, 52 (2003).
[11] Z. Wang, W. Jury, A. Tuli, and D.-J. Kim, Vadose Zone J. **3**, 549 (2004).
[12] L. A. Richards, Physics (N.Y.) **1**, 318 (1931).
[13] M. Eliassi and R. Glass, Water Resour. Res. **37**, 2019 (2001).
[14] G. Diment, K. Watson, and P. Blennerhassett, Water Resour. Res. **18**, 1248 (1982).
[15] G. Diment and K. Watson, Water Resour. Res. **19**, 1002 (1983).
[16] V. Kapoor, Transp. Porous Media **25**, 313 (1996).
[17] N. Ursino, Transp. Porous Media **38**, 261 (2000).
[18] A. Egorov, R. Dautov, J. Nieber, and A. Seshukov, Water Resour. Res. **39**, 1266 (2003).
[19] C. van Duijn, G. Pieters, and P. Raats, Transp. Porous Media **57**, 215 (2004).
[20] J. Nieber, R. Dautov, A. Egorov, and A. Sheshukov, Transp. Porous Media **58**, 147 (2005).
[21] P. G. Saffman and G. I. Taylor, Proc. R. Soc. London, Ser. A **245**, 312 (1958).
[22] R. L. Chuoke, P. van Meurs, and C. van der Poel, Trans. Am. Inst. Min., Metall. Pet. Eng. **216**, 188 (1959).
[23] D. A. Weitz, J. P. Stokes, R. C. Ball, and A. P. Kushnick, Phys. Rev. Lett. **59**, 2967 (1987).
[24] D. A. DiCarlo and M. J. Blunt, Water Resour. Res. **36**, 2781 (2000).
[25] B. Xu, Y. C. Yortsos, and D. Salin, Phys. Rev. E **57**, 739 (1998).
[26] B. Berkowitz and R. P. Ewing, Surv. Geophys. **19**, 23 (1998).
[27] S. Geiger and D. Durnford, Soil Sci. Soc. Am. J. **64**, 460 (2000).
[28] D. DiCarlo, Water Resour. Res. **40**, W04215 (2004).
[29] S. Shiozawa and H. Fujimaki, Water Resour. Res. **40**, W07404 (2004).
[30] D. DiCarlo, Water Resour. Res. **43**, W08402 (2007).
[31] G. I. Barenblatt, T. W. Patzek, and D. B. Silin, SPEJ **8**, 409 (2003).
[32] D. A. DiCarlo, R. Juanes, T. LaForce, and T. P. Witelski, Water Resour. Res. **44**, W02406 (2008).
[33] W. Gray and S. Hassanizadeh, Water Resour. Res. **27**, 1847 (1991).
[34] S. Hassanizadeh and W. Gray, Water Resour. Res. **29**, 3389 (1993).
[35] C. Cuesta, C. van Duijn, and J. Hulshof, Eur. J. Appl. Math. **11**, 381 (2000).
[36] M. Eliassi and R. Glass, Water Resour. Res. **38**, 1234 (2002).
[37] M. Eliassi and R. Glass, Water Resour. Res. **39**, 1167 (2003).
[38] J. Krug and P. Meakin, Phys. Rev. Lett. **66**, 703 (1991).
[39] L. Antanovskii, Phys. Fluids **7**, 747 (1995).
[40] M. Dubé, M. Rost, K. R. Elder, M. Alava, S. Majaniemi, and T. Ala-Nissila, Phys. Rev. Lett. **83**, 1628 (1999).
[41] L. Cueto-Felgueroso and R. Juanes, Phys. Rev. Lett. **101**, 244504 (2008).
[42] H. E. Huppert, Nature (London) **300**, 427 (1982).
[43] A. Bertozzi and M. Brenner, Phys. Fluids **9**, 530 (1997).
[44] J. Cahn, Acta Metall. **9**, 795 (1961).
[45] J. Cahn and J. Hilliard, J. Chem. Phys. **28**, 258 (1958).
[46] A. Karma and W.-J. Rappel, Phys. Rev. Lett. **77**, 4050 (1996).
[47] H. Emmerich, Adv. Phys. **57**, 1 (2008).
[48] J. Davis and S. Troian, Phys. Fluids **15**, 1344 (2003).
[49] J. Davis, D. Kataoka, and S. Troian, Phys. Fluids **18**, 092101

(2006).
[50] T. P. Witelski, A. J. Bernoff, and A. L. Bertozzi, Eur. J. Appl. Math. **15**, 223 (2004).
[51] L. Trefethen, A. Trefethen, S. Reddy, and T. Driscoll, Science **261**, 578 (1993).
[52] B. Farrell and P. Ioannou, J. Atmos. Sci. **53**, 2025 (1996).
[53] L. Trefethen and M. Embree, *Spectra and Pseudospectra* (Princeton University Press, Princeton, 2005).
[54] J. S. Selker, J.-Y. Parlange, and T. Steenhuis, Water Resour. Res. **28**, 2523 (1992).
[55] T. X. Lu, J. W. Biggar, and D. R. Nielsen, Water Resour. Res. **30**, 3283 (1994).
[56] J. Bear, *Dynamics of Fluids in Porous Media* (Elsevier, New York, 1972).
[57] J. R. Philip, in *Advances in Hydroscience*, edited by V. T. Chow (Academic Press, New York, 1969), pp. 215–296.
[58] M. C. Leverett, Trans. Am. Inst. Min., Metall. Pet. Eng. **142**, 152 (1941).
[59] P. G. de Gennes, Rev. Mod. Phys. **57**, 827 (1985).
[60] Y. Mualem, Water Resour. Res. **12**, 513 (1976).
[61] M. van Genuchten, Soil Sci. Soc. Am. J. **44**, 892 (1980).
[62] T. Tee and L. Trefethen, SIAM J. Sci. Comput. (USA) **28**, 1798 (2006).
[63] L. Cueto-Felgueroso and R. Juanes (unpublished).